Atmos. Chem. Phys. Discuss., 9, 10829–10881, 2009
www.atmos-chem-phys-discuss.net/9/10829/2009/

Atmospheric Chemistry and Physics Discussions

This discussion paper is/has been under review for the journal *Atmospheric Chemistry and Physics (ACP)*. Please refer to the corresponding final paper in *ACP* if available.

Bacteria in the global atmosphere – Part 2: Modelling of emissions and transport between different ecosystems

S. M. Burrows, T. Butler, P. Jöckel, H. Tost, A. Kerkweg, U. Pöschl, and M. G. Lawrence

Max Planck Institute for Chemistry, Mainz, Germany

Received: 6 March 2009 – Accepted: 30 March 2009 – Published: 4 May 2009

Correspondence to: S. M. Burrows (susannah.burrows@mpic.de)

Published by Copernicus Publications on behalf of the European Geosciences Union.

Abstract

Bacteria are constantly being transported through the atmosphere, which may have implications for human health, agriculture, cloud formation, and the dispersal of bacterial species. We simulated the global transport of bacterial cells, represented as 1 μm diameter spherical solid particle tracers, in a chemistry-climate model. We investigated the factors influencing residence time and distribution of the particles, including emission region, CCN activity and removal by ice-phase precipitation. The global distribution depends strongly on the assumptions made about uptake into cloud droplets and ice. The transport is also affected, to a lesser extent, by the emission region and by season. We examine the potential for exchange of bacteria between ecosystems and obtain rough estimates of the flux from each ecosystem by using an optimal estimation technique, together with a new compilation of available observations described in a companion paper. Globally, we estimate the total emissions of bacteria to the atmosphere to be 1400 Gg per year with an upper bound of 4600 Gg per year, originating mainly from grasslands, shrubs and crops. In order to improve understanding of this topic, more measurements of the bacterial content of the air will be necessary. Future measurements in wetlands, sandy deserts, tundra, remote glacial and coastal regions and over oceans will be of particular interest.

1 Introduction

The transport of microorganisms in the atmosphere could have important implications for several branches of science, including impacts on human health, agriculture, clouds, and microbial biogeography (Burrows et al., 2009). Unravelling these effects has been difficult, partly because so little is known about the concentrations and sources of atmospheric microorganisms, as well as their transport pathways.

Bacteria are aerosolized from virtually all surfaces, including aerial plant parts, soil and water surfaces (Gregory, 1973; Jones and Harrison, 2004). They can be removed

ACPD

9, 10829–10881, 2009

from surfaces by gusts of wind or mechanical disturbances, such as shaking of leaves or surf breaking. Upon entering the air, they can be transported upwards by air currents and remain in the atmosphere for an average period of a few days. They are eventually removed from the atmosphere by either "dry" deposition – adherence to buildings, plants, the ground and other surfaces in contact with the air – or "wet" deposition – the precipitation of rain, snow or ice that has collected particles while forming or while falling to the surface.

The potential for bacteria and other microorganisms to be transported over long distances through the air has long fascinated microbiologists and been a focus of the field of aerobiology. The average residence time of microorganisms in the atmosphere can range from several days to weeks, long enough for cells to travel between continents. Many microorganisms have defense mechanisms which enable them to withstand the environmental stresses of air transport, including exposure to UV radiation, dessication, and low pH within cloud water, so some microorganisms survive this long-range transport to new regions and arrive in a viable state.

We focus on the transport of bacteria through the air on global scales. Using a general circulation model to simulate particle transport (Sect. 2), we investigated the rate of transfer of bacteria-sized particles between various ecosystems. We estimated the emissions of bacteria from ten lumped ecosystem classes as a first step towards a simple model of emissions of biological particles to the atmosphere. An additional advantage of this approach is that it allows us to investigate the transfer of genetic material between ecosystems, which has important implications for microbial biogeography. We give quantitative estimates of inter-ecosystem transport of bacteria, and show that it can be very large for some regions.

By adjusting the simulation results to observed concentrations, we estimated the rate at which bacteria are transferred from land surfaces to the atmosphere. A realistic estimate of emission rates is an important step towards modelling realistic distributions in various regions.

Our results suggest that in some regions, the concentration of bacteria in the upper

troposphere could be similar to typical concentrations of atmospheric ice nuclei. Although most bacteria are not ice-nucleation active, this result suggests that the potential for bacteria to play a significant role in ice nucleation deserves further investigation. Several investigators have used cloud microphysical models and cloud-resolving models to study the potential effects of bacteria on cloud development, but results of such studies so far are inconclusive (Diehl et al., 2006; Möhler et al., 2007).

2 Model description

We simulated particle transport using the EMAC model (ECHAM5/MESSy1.5 Atmospheric Chemistry). EMAC is a model system consisting of the atmospheric general circulation model ECHAM5 (Roeckner et al., 2003), coupled to various subprocess models via the Modular Earth Submodel System (MESSy) interface (Jöckel et al., 2005; Jöckel et al., 2006). The system can be used to simulate both weather and climate, and study their effects on atmospheric chemistry and tracer transport. The model is available to the community (see http://www.messy-interface.org).

We simulated the transport of aerosol tracers of 1 μm diameter and 1 g cm^{-3} density. A separate tracer was emitted from each of ten lumped ecosystem classes. Bacteria were emitted homogeneously within each region. This allowed us to determine the fate of particles from each ecosystem source region.

The model ran in T63L31 resolution for six simulated years without nudging of wind fields or other data assimilation. Initial meteorological fields were derived from the ECMWF ERA-15 reanalysis for 1 January 1990. Monthly prescribed sea surface temperature were taken from the AMIP-II data set (Available from http://www-pcmdi.llnl.gov/). Initially, no bacteria were present in the air. The global atmospheric burden of the simulated bacteria reached quasi-equilibrium within the first three simulated years (spin-up). The analysis was conducted using climatological averages of the bacterial distribution during the last three years of the simulation.

The simulations included parameterizations of wet and dry removal processes, as

well as transport by advection and parameterized convection. A detailed description of the model set-up is included in Appendix A.

The ecosystem classification was based on the Olson World Ecosystems dataset (Olson, 1992) and is described in detail in Appendix B, Table B1. The choice of lumped ecosystem groups necessarily involves compromises. For the lumping used here, taigas were grouped with tundras, since both are boreal, cold and usually frozen regions. However, some other snowy or boreal forests were grouped with forests, a group that also includes forests in tropical, sub-tropical and moderate climates. Other ambiguous ecosystem types include rice paddies (which could be considered crops or wetlands), mangroves and tidal mudflats (wetlands or coastal), and the various mixed vegetation areas (such as field/woods types). Given the current limited state of knowledge regarding the emissions and distribution of bacteria in the air, it seemed appropriate to limit the number of lumped classes to a reasonably small number.

3 Sensitivity of modeled tracer transport to source ecosystem and scavenging characteristics

Three model simulations were performed using different scavenging characteristics to investigate the effects of scavenging processes on bacteria transport and lifetime. Losses to dry deposition, and to scavenging by impaction and interception were included in all three simulations, while CCN activity and ice phase scavenging were varied among the three sensitivity simulations: CCN-ACTIVE, CCN-INACTIVE and NO-ICE-SCAV (Table 1).

3.1 Global load and atmospheric lifetime

The mean global loads and lifetimes calculated for the three model simulations are given in Table 2. The lifetime of a few days for CCN-ACTIVE and CCN-INACTIVE bacteria is consistent with theoretical expectations for particles of 1 μm diameter (Roedel,

1992). In contrast, the long lifetimes of about 100 days for bacteria in the NO-ICE-SCAV simulation is unrealistically long.

3.1.1 Dependence of the global mean lifetime on source region and season

The global mean atmospheric lifetime of bacteria varies depending on the source region (Table 2) and on season, due mainly to differences in transport and precipitation patterns (Fig. 2).

Without ice phase scavenging, the mean lifetime is on the order of months, and the global NO-ICE-SCAV load varies relatively little during the year. In the CCN-INACTIVE simulation, particles originating in deserts, shrubs, grasslands, and coastal regions have the longest residence times, along with tundra and land ice particles during the austral summer. Several of these ecosystems – deserts, shrubs, and grasslands – are predominantly located in drier, often tropical climates. Uptake into tropical convective systems and transport to the upper troposphere is likely, and low levels of precipitation in the source region result in slower removal, and long particle lifetimes. Particles emitted in these regions are therefore more likely to participate in long-distance transport. Indeed, the long-distance transport of dust from warm deserts has long interested meteorologists. Bacteria are known to attach to dust particles and are routinely transported over long distances within dust clouds, where the attenuation of UV radiation by the cloud is believed to improve chances of survival (Griffin et al., 2001a,b).

The source ecosystems with the shortest particle lifetimes in the CCN-INACTIVE simulation are seas, tundra during the austral winter and spring, and forests.

Compared to the CCN-INACTIVE simulation, the lifetimes in the CCN-ACTIVE simulation are shorter by a factor of about 1.5 to 2. Also, the effect of season on lifetime is different, particularly for the land ice and tundra tracers.

3.2 Mean column density

The mean column density of the total bacteria is shown in Fig. 3. The CCN-INACTIVE and CCN-ACTIVE simulations, which both include ice phase scavenging, show very similar geographic distributions, with slightly higher concentrations in the CCN-INACTIVE simulation. In these two simulations, column densities are highest in polar regions, consistent with the long lifetime of the land ice and tundra tracers (Fig. 2). High column densities in sub-Saharan Africa and northwestern Australia coincide with arid regions dominated by grasslands, shrubs and deserts, consistent with long particle lifetimes (deserts, shrubs) and large relative vertical transport rates (grasslands).

In the third simulation, NO-ICE-SCAV, column densities are much greater and more homogeneous, consistent with the much longer lifetimes of particles in this simulation (Fig. 2). In the absence of efficient scavenging, the column densities are highest in the tropics, probably due to strong convective lifting, resulting in a longer lifetime. This interpretation is supported by studies of dust transport such as Schulz et al. (1998) which showed that satellite observations of dust plumes could only be reproduced with a combination of the correct localization of source regions, rapid upward transport by convective updrafts and horizontal transport at upper altitudes.

4 Inversion

This section discusses the estimation of bacterial emissions in each ecosystem class based on a synthesis of literature results (Table 3) and model results. The analysis is based on output from the CCN-ACTIVE simulation, which has the most realistic scavenging characteristics, including both CCN scavenging and ice-phase scavenging.

Using literature estimates, we adjust the emissions of bacteria from each ecosystem to achieve a simulated distribution of airborne bacteria that is more representative of available observations. When sufficient information is available about the distribution of an atmospheric trace compound or aerosol, sophisticated inverse modelling

techniques can be used to estimate sources (e.g. Kasibhatla et al., 2000). Given the paucity of data on bacterial concentrations, it seems reasonable to instead take a simpler approach to obtain some first estimates of the global sources and distribution. Our results give a starting point for further studies, and will be subject to modification and improvements as more measurements become available.

4.1 Observed concentrations

Our concentration estimates are presented in Table 3 and discussed in detail in a companion paper (Burrows et al., 2009). They are based mainly on the seven field studies listed in the footnotes of Table 3. Values are based on average concentrations of airborne bacteria as observed over a period of a few days to a few weeks. In four of these studies, only the culturable bacteria were observed. Culturable bacteria are typically measured by collecting aerosol samples on a nutrient agar and counting the number of colonies that form during subsequent incubation. In environmental aerosol samples, the culturable bacteria are typically about 1% of the total aerosol sample, although this fraction also depends on environmental and experimental variables (Burrows et al., 2009). In three studies, total atmospheric bacteria were observed (Tong and Lighthart, 1999; Bauer et al., 2002; Harrison et al., 2005). Total bacteria can be counted by staining proteins in an aerosol sample with a fluorescent dye, and then counting the number of bacteria in a sample under a microscope.

Observations are very sparse and even non-existant in some regions. To perform the analysis, we made some additional assumptions about concentrations beyond those discussed in (Burrows et al., 2009). These are indicated by italic font and parentheses in Table 3, and explained in the footnotes to the table.

4.2 Mathematical considerations

In the present model, bacteria sources are constant and sinks depend linearly on the bacteria concentration. It follows that the adjusted bacteria mixing ratio x_{mijkt} in

ecosystem m is given by a linear combination of the emission factors f_n in the N ecosystems, weighted by a tensor W_{nijkt} (the indices i, j, k and t designating the model grid point in longitude, latitude, altitude, and time for each ecosystem m, respectively):

$$x_{mijkt} = \sum_{n=1}^{N} W_{nijkt} f_n. \quad (1)$$

The tensor W_{nijkt} is simply the distribution of bacteria from ecosystem n. Due to the limited number of observations, the focus here will be only on values in the lowest model level, averaged in latitude, longitude and time, in which case Eq. (1) becomes

$$\overline{x}_m = \sum_{n=1}^{N} \overline{W}_{nm} f_n, \quad (2)$$

or, in vector notation,

$$\overline{\mathbf{x}} = \overline{\mathbf{W}}\mathbf{f}. \quad (3)$$

The weighting function $\mathbf{W}$ can be calculated directly from the model results for emission at 1 m^{-2} s^{-1}. The weights $\overline{W}_{nm}$ are then given by

$$\overline{W}_{nm} = \overline{x}_{nm}, \quad (\mathbf{f} = \mathbf{1}) \quad (4)$$

where x_{nm} is the mean concentration of the tracer from ecosystem n in ecosystem m. Using these weights, which can be calculated from a single simulation, we can calculate the distribution that would result from any arbitrary set of emission factors, (f_n). The inverse model can also be obtained directly from $\overline{\mathbf{W}}$: if the emission factors f_n are allowed to take on arbitrary real values, Eq. (3) has an exact solution (provided the matrix $\overline{\mathbf{W}}$ is non-singular). It is also possible to find a best-fit solution under specific constraints, such as requiring the fluxes f_n to be non-negative. Conceptually, this approach amounts to reducing the output of the global climate model to a ten-box equilibrium model. Mathematically, the approach is equivalent to Green's function synthesis (Enting, 2000).

4.3 Discussion of the calculated weighting matrix and ecosystem cross-correlations

We calculated the weighting matrix **W** for the simulated near-surface concentrations of the CCN-ACTIVE simulation (Table C1, Figs. 4, 5, and 6). Each row of Table C1 gives the mean concentrations of all ecosystems tracers found in the near-surface air of a single destination ecosystem class, for homogeneous aerosol emissions of $1\,m^{-2}\,s^{-1}$.

Some ecosystems have similar transport pathways and deposition footprints, resulting in high correlations between the columns of **W**. We computed the cross-correlations of the columns of **W** (Table C4 and Fig. 4). A large positive correlation between two ecosystems means that the distribution of the source ecosystem tracer among the ten ecosystem classes is similar, as is likely to occur for geographically adjacent regions. Notable positive correlations occur between seas and coastal regions, which are always contiguous, and between desert and shrub regions, which are almost always contiguous (Fig. 1). All other large positive correlations (correlation>0.4) involve the forest ecosystem tracer, whose distribution is positively correlated with the distributions of the crops, grasslands, and wetland tracers. Inspection of Fig. 1 shows that these ecosystems are indeed often found adjacent to forested regions.

A large cross-correlation between the distributions of two ecosystem tracers means that the tracer distributions are significantly linearly dependent on each other. This could point to weaknesses in the ecosystem lumping. For example, for future studies it may be more meaningful to combine the coastal and seas regions, while splitting the forests into several groups that more accurately reflect the diversity of forested ecosystems. A sensible alternate subdivision, however, would ideally also take into account the availability of observations.

4.4 Numerical fitting procedures

The exact solution of Eq. (3) results in negative surface fluxes for some ecosystems and negative simulated total concentrations at some locations. Therefore, in addition to the

ACPD
9, 10829–10881, 2009

exact solution, we fit the data iteratively while constraining fluxes to be non-negative.

A first adjustment was done by hand to obtain a set of fluxes that meets this criterion, for the purposes of numerical optimization. Then a "best" fit (in a maximum likelihood sense) for the fluxes was obtained by using a constrained optimization technique.

4.4.1 Constrained weighted least squares fitting – Method 1

The solution was found by minimizing the weighted sum of the squared differences between modelled and literature fluxes:

$$\sum_{n=1}^{N} \frac{(x_n - \text{goal}_n)^2}{\text{high}_n - \text{low}_n}, \tag{5}$$

where goal_n is the fitting goal (literature estimate), subject to the constraint $f_n \geq 0\,\text{m}^{-2}\,\text{s}^{-1}$. The weighting term $(\text{high}_n - \text{low}_n)^{-1}$ reflects the uncertainty associated with each literature estimate. Best-fit fluxes were calculated individually using the low, best and high literature estimates as the goal.

The minimization of the unweighted least-squares fit was also tested (results not shown). In the unweighted case, the highest estimated concentrations (grasslands, shrubs) were fitted with high precision, while the fits for other ecosystems (such as forests and deserts) were relatively much poorer. The high-concentration regions dominated the fitting procedure such that the concentrations in other regions were seriously overestimated. Using the weighted cost function (Eq. 5) mitigates this problem, since regions with higher concentrations also tend to have greater associated absolute uncertainties.

4.4.2 Maximum likelihood fitting – Method 2

A second, more sophisticated fitting procedure was also applied in which modelled concentrations outside the range of maximum and minimum estimated values were penalized.

The following cost function was minimized:

$$\sum_{n=1}^{N} \frac{(x_n - \text{goal}_n)^2}{(\text{high}_n - \text{low}_n)} + \mu \cdot (\exp(\text{low}_n - x_n) + \exp(x_n - \text{high}_n)), \quad (6)$$

where μ is a scaling term for the boundary penalty, set to μ=0.001, which is several orders of magnitude smaller than the first term in Eq. (6) for the values we used (given in Table 3). Maximum-likelihood parameters were calculated for the minimum, mean, and maximum literature values, subject to the constraint $f_n \geq 0\,\text{m}^{-2}\,\text{s}^{-1}$.

4.5 Results

For the iterative optimization routines, an initial guess was selected by hand that satisfied the upper and lower bounds on the mean concentration (the high and low literature estimates) and the lower bound on the fluxes ($f_n \geq 0$) for each ecosystem. The fitted fluxes and the initial guess used in the numerical routines are listed in Table C3, while the modelled concentrations resulting from those fluxes are listed in Table C2. Additionally, the estimated fluxes and resultant concentrations are illustrated in Fig. 7.

The exact solution of Eq. (3) for the literature best estimate of concentrations is listed in Table C3[1]. For five of the ten ecosystem groups, the estimated mean fluxes are negative, and at some locations, the resulting total bacterial concentrations are negative (not shown). Physically, concentrations can not be negative, and fluxes may be negative only if the model underestimates deposition (because modelled particle sinks are implicitly included in the weighting matrix **W**). If the concentrations being fitted had high precision, such a result could point to problems with the model, such as a failure to accurately represent all model sinks. However, in the present case the

[1] In contrast to the maximum likelihood fits, the exact solution does not depend on an initial guess, and the agreement of the exact solution flux with the initial guess for the land ice tracer is coincidental.

model transport and sink processes probably have a higher level of confidence than the highly uncertain literature estimates of bacterial aerosol concentrations.

In constrained fits ($f>0$), an exact fit to the best guess concentration cannot be attained, but the initial guess and the results of both fitting routines each produce concentrations within the bounds of literature estimates for each of the ten ecosystem classes (Fig. 7). The two fitting routines obtain similar results, with the exception of emissions from wetlands, which are $510\,m^{-2}\,s^{-1}$ in the Method 1 fit, and 0 in the Method 2 fit. The effect of this difference on the resulting concentrations is small, as could be anticipated considering the small impact of wetland emissions on concentrations elsewhere (Table C1).

The constrained iterative calculation of the best fit results in emissions greater than zero in only a few regions. The Method 2 best fit requires emissions from only four of ten ecosystem groups: grasslands, crops, shrubs and land ice. The Method 1 best fit additionally includes emissions from wetlands. With the exception of land ice, these are the ecosystems with the highest estimated bacterial concentrations. Fitted concentrations are lower than literature estimates in three regions (grasslands, crops, and shrubs), higher in five regions (coastal, deserts, forests, seas, and tundra) and close matches in two regions (land ice and wetlands). This observation makes clear why in certain regions, the estimated flux is zero in constrained fits and negative in unconstrained fits. The emissions of grasslands, crops, and shrubs are fitted to values which are not high enough to allow concentrations to be matched in the respective ecosystems. However, these tracers are exported to other ecosystems, such as deserts, in sufficient quantities that the literature estimates there are exceeded (Table C1). Additional emissions from a region in which estimates are already exceeded would result in an even greater overshoot, further increasing the distance between the simulated concentrations and the goal. The high emissions in grassland, crop, and shrub regions are a result of the numerical compromise between the competing goals of fitting high concentrations in those ecosystems and low concentrations elsewhere.

The land ice region is an unusual case, since it is essentially dynamically decoupled

from the other ecosystem classes. The land ice ecosystem class is dominated by the Antarctic continent. The isolation of the continent from other land types is exacerbated in winter by the formation of the polar vortex. The result is a relatively small exchange of tracers with the seas, and virtually zero tracer exchange with other land ecosystems (Table C1). In addition, particles emitted here have a long lifetime (Fig. 2), so despite low emission estimates, more than 90% of the aerosol found in the land ice regions is estimated to originate in that region.

In all other regions, contributions from the crop, grassland, and shrub tracers dominate, with these three sources making up about 80–90% or more of the near-surface load. An interesting feature is the high percentage of aerosol over the tundra that originates in agricultural areas. While tundra regions tend to be adjacent to forests and seas, these do not emit particles in the fitted model. Grasslands and shrubs, the other major emitters, are concentrated in warmer climates, and are thus often farther from tundra than agricultural areas.

Uncertainties were explored empirically by performing the inversion for an ensemble of vectors with elements taken from the low, middle and high concentration estimates for each region (Fig. 8; see caption for details of the eensemble simluations). When fluxa values are unconstrained, Method 2 reproduces the exact solution, while Method 1 produces a different distribution with larger variability. This likely indicates that the Method 1 solution algorithm is more likely to be caught in a local minimum, while the Method 2 constraint places a stronger penalty on solutions for which the concentrations exceed the bounds of the estimated region, and is thus less likely to stray from the exact solution. Thus, Fig. 8 shows only the Method 2 solutions for constrained and unconstrained minimization.

Forcing the flux to be positive is equivalent to an a priori assumption that particle deposition is simulated accurately. However, when negative fluxes are allowed, flux estimates in both forests and coastal regions are negative. A possible explanation is that model parameterizations underestimate particle deposition in these regions.

The model predicts low emissions of bacteria from seas, a result which appears to

be robust. The largest uncertainties are found in wetlands and coastal regions, ecosystems with small land areas, which contribute little to the particle content of the air elsewhere. Thus, the emissions in these regions are poorly constrained by concentration estimates elsewhere.

Taking the median of the ensemble as the best estimate and the 5%ile–95%ile range as an uncertainty estimate, we obtain about 1400 (22–4050) Gg year^{-1} for the exact solution and about 690 (402–1488) Gg year^{-1} for the Method 2 solution with the constraint that fluxes must be $\geq$0 (an overview of the percentile results is given in Appendix C, Tables C5 and C6). Because the positive constraint implies greater a priori knowledge than is available, we use the results of the exact solution ensemble as a best estimate of the global emissions.

5 Analysis of adjusted model results

After adjusting the emissions to the Method 2 best fit values, the modelled particle distribution was recalculated. The total emissions from each of the ecosystems in the adjusted results are shown in Table 4. These emissions result in new patterns of particle distribution, with some differences to the distributions found in the homogeneous emissions case.

5.1 Distribution

5.1.1 Horizontal distribution

The change from homogeneous to adjusted emission fluxes results in a strong shift in the surface concentrations away from the polar regions and oceans, towards tropical regions and land (Fig. 9). The regions of high vertical column density, however, are similar in the two cases. The regions with high estimated emission fluxes (grasslands, shrubs and crops) are also among those with the most efficient vertical transport and

longest particle lifetimes. This means that they have a much larger impact on the vertical column density relative to their surface concentrations than the land ice or tundra tracers, which remain trapped near the surface.

5.2 Estimated global load and annual emissions

Overall diagnostics comparing the homogeneous emissions case and the adjusted emissions case (using the Method 2 best fit) were calculated (Table 5). The elimination of emissions from seas and oceans results in an increased difference between higher concentrations over land and lower concentrations over the seas. The global mean tracer lifetime is longer for the adjusted emissions case (5.5 days) than for the homogeneous emissions case (3.3 days).

For adjusted emissions, the estimated mean global load of bacterial cells is 1.7×10^{22}. Assuming spherical bacteria of 1 μm diameter and a density of 1 g cm^{-3}, the mass of one cell is 0.52 pg and the total bacterial mass is approximately 9.0 Gg. The total estimated emission of bacterial cells from land surfaces is about 250 m^{-2} s^{-1}, resulting in total annual emissions of about 1.2×10^{24}, or about 610 Gg. This is only a very small fraction of the estimated total PBAP source of 1000 Tg/year (Jaenicke, 2005).

By comparison, Elbert et al. (2007) estimate that globally, fungal spores are emitted from land surfaces at an average rate of 200 m^{-2} s^{-1} over land, comparable to these results. However, with a mean assumed diameter of 5 μm, a fungal spore has a mass of about 65 pg, 125 times greater than the approximately 0.52 pg we assume for bacteria. Together, this results in a global fungal spore burden of about 140 Gg and a source of about 50 Tg per year. For the larger fungal spores, Elbert et al. (2007) assume a mean residence time of 1 day, while the bacteria we simulated have a mean residence time of 5.5 days.

ACPD
9, 10829–10881, 2009

5.3 Limitations and sources of uncertainty

The approach taken here amounts to the reduction of the global emission and transport of particles to a ten-box system, with sink processes and exchange between the boxes implicitly contained in the weighting matrix (Table C1). This approach allows useful insights to be gained into a problem for which the level of knowledge is, at present, very low. However, such an approach has limitations, including the following:

- The ecosystem classification chosen involves various compromises (as discussed in Sect. 2) and some ecosystem classes may not be well-defined for the current purposes. For example, considering the high positive correlation of the coastal and seas tracer distributions (Table C4 and Fig. 4), it might be reasonable to combine these groups. The forest group, on the other hand, includes a variety of diverse regions, and in a future study it might be more meaningful to distinguish between the various types of forest ecosystems.

- Most of the literature estimates are based on a single study or on assumptions about the similarities among ecosystem types. Even in well-studied land types (such as croplands), the variability between sites is high, and the sites studied may not be representative of the entire class.

- Emissions of bacteria are likely to depend on temperature, wind, and other meteorological variables (Jones and Harrison, 2004; Burrows et al., 2009), effects not considered in the current study. This may have important consequences for distributions (due, for instance, to differences between daytime and nighttime transport).

- The iterative fitting methods described in Sect. 4.4 may not produce unique solutions for the current problem.

- We consider spherical particles with a uniform diameter of 1 μm, a typical size for bacterial cells – *E. coli*, for instance, is 1.1 to 1.5 μm wide by 2.0 to 6.0 μm

long (Prescott et al., 1996). However, bacterial diameters can range from about 100 nm to as much as 750 μm, and cells come in a variety of shapes (Schulz and Jorgensen, 2001). The size and shape of a bacterium will strongly affect its atmospheric lifetime.

In spite of these limitations, our approach takes advantage of the limited available experimental data to yield first guesses of many values that so far have remained unquantified. This work provides a framework for the interpretation and incorporation of future experimental findings.

6 Summary and conclusions

6.1 Model results: particle transport characteristics

Using a global chemistry-climate model, we investigated the transport of bacteria in the atmosphere and its sensitivity to scavenging and the source ecosystem. While the ecosystem approach was applied here specifically to study emissions of bacteria, it also results in significant general learning about the differences in transport experienced by particles emitted from various ecosystems, and thus may be applicable to other natural organic aerosols.

We estimate the mean global atmospheric lifetime of a homogeneously emitted bacteria tracer to be about 2.5 days for the CCN-ACTIVE simulation, 5 days for CCN-INACTIVE, and several months for NO-ICE-SCAV. These lifetimes are long enough for significant long-distance transport to occur in the atmosphere. For tracers with the same scavenging characteristics, the lifetime varies significantly as a function of emission region.

ACPD
9, 10829–10881, 2009

6.2 Estimation of global emissions of bacterial aerosol

The results of a literature review (Burrows et al., 2009) and the modeling study were synthesized to obtain a better understanding of the global distribution of bacteria in the atmosphere. Using a maximum likelihood estimation procedure, we estimated emission rates for each of ten ecosystem types. The mean continental emissions of bacteria were estimated to be about 250 cells m^{-2} s^{-1} or 610 Gg $year^{-1}$ by an iterative method with fluxes constrained to be positive. By estimating the emissions for an ensemble of estimated concentrations, we obtain total global emissions of 1400 (20–4000) Gg $year^{-1}$ (median and 5%ile–95%ile), consistent with literature measurements showing concentrations to be about 10^4–10^5 m^{-3} in most regions. This is, based on the broad range of literature reviewed, the first estimate of global bacterial emissions to the atmosphere.

The estimated emissions are of the same order of magnitude by number as fungal spore emissions, which Elbert et al. (2007) estimated to be about 200 m^{-2} s^{-1}. The mass flux, however, is much smaller than the 50 Tg/year estimated for total fungal spores, because the mass of a bacterium, assumed here to be 0.52 pg/cell, is much smaller than that of a single spore, assumed by Elbert et al. (2007), to be 65 pg. The estimate of fungal spore emissions by Elbert et al. (2007), in turn, is small compared to the the 1000 Tg/year (Jaenicke, 2005) that have been estimated for the total emission of primary biological aerosol particles.

Sources of bacteria in the adjusted simulation were mainly restricted to the regions with the highest estimated bacterial concentrations (grasslands, shrubs and crops). Strong emissions in those regions meant that particles were exported in quantities large enough to exceed estimated mean concentrations elsewhere.

6.3 Outlook

Many open questions remain with respect to the role of bacteria in the atmosphere, including:

– How important is “continuous” vs. “intermittent” transport of bacteria (e.g. Wolfenbarger, 1946)?

– How do bacteria influence cloud formation? Does the presence of bacteria affect precipitation or the radiative properties of clouds as part of a larger feedback cycle (the “bioprecipitation” hypothesis) (Schnell and Vali, 1973; Sands et al., 1992; Bauer et al., 2003; Morris et al., 2005; Sun and Ariya, 2006)?

– To what degree are bacteria able to reproduce in the atmosphere? Does the atmosphere provide a niche for particular microorganisms (Dimmick et al., 1979; Sattler et al., 2001; Amato et al., 2007)?

– Does the degradation of organic compounds by bacteria play a significant role in the chemistry of liquid particles in the atmosphere (Herlihy et al., 1987; Ariya, 2002; Amato et al., 2007)?

The answer to each of these questions either depends on or enhances our knowledge of atmospheric bacterial concentrations. Quantifying the distribution of atmospheric bacteria will therefore remain an important goal of investigators seeking to understand interactions between bacteria and the atmospheric environment. Attention should be paid to quantifying total (as opposed to culturable) bacterial concentrations, emission fluxes and vertical profiles. Flux measurements of total bacteria are especially important for improving understanding of the origins of airborne bacteria.

Past measurements of ambient bacterial concentration have tended to focus on urban sites and point sources, or on emissions from agricultural sources. As a result, many ecosystems have been neglected, especially those that are not easily accessible to researchers. Ecosystem types for which no published measurements of airborne bacterial concentrations were found include tropical rain-forests, wetlands, sandy deserts, tundra, and glaciated regions. Also, few measurements have been made over oceans and seas. Measurements of the total concentration, flux and ice-nucleating properties of bacteria over biologically active regions of the oceans would help to clarify

whether the marine source makes a significant contribution to the high IN concentrations observed in these regions as argued by Schnell and Vali (1976).

Further laboratory measurements are needed to investigate the activity of bacteria in droplet and ice crystal formation. While it is clear that some bacteria are highly effective ice nucleators, it remains unclear what percentage of environmental bacteria are INactive or how to treat the CCN activity of environmental bacteria (CCN activities have been measured by Bauer et al., 2003 and Franc and DeMott, 1998). Studies addressing uptake into cloud and rain droplets would help to quantify scavenging efficiency for bacterial cells, and the potential effect of hydrophobic cell surfaces on uptake.

The microbiology of the atmosphere is a topic that presents challenges and opportunities for many disciplines. Atmospheric transport models can make a useful contribution to understanding the sources and distribution of bacteria in the atmosphere. However, there is a need for more measurements, particularly measurements of total (as opposed to viable) bacterial concentrations and fluxes, if further progress it to be made. Because of the many gaps in current knowledge of atmospheric microflora, this study can not be considered complete. Nevertheless, it is expected that the global overview obtained from the current approach, and the estimates of the mean global emissions and concentrations, should be useful in assessing the likely magnitude of effects resulting from the presence of bacteria in the air.

Appendix A Model setup and data handling

A1 Tracers in EMAC

In the EMAC system, the back-end for consistent handling of atmospheric constituents is the generic submodel TRACER (Jöckel et al., 2008), which includes two sub-submodels, TRACER_FAMILY and TRACER_PDEF. The sub-submodel TRACER_FAMILY was used to correct small nonlinearities in tracer advection due to operator splitting. The sub-submodel TRACER_PDEF corrects small negative values

due to numerical overshoots. The submodel PTRAC was used to define the tracers and their characteristics, including size, density, and CCN activity.

Tracer advection is calculated in EMAC using the Lin and Rood (1996) integration algorithm, which is mass-conserving, linear, and monotonic in its 1-D form.

The EMAC submodel ONLEM (Kerkweg et al., 2006b,c) enables flexible online calculation of tracer emissions based on a combination of geographical data (e.g. land cover or soil type) and/or current meteorological conditions. ONLEM was extended by a subroutine to simulate the emission of the bacteria tracer.

Sedimentation and other dry deposition processes are simulated by the MESSy submodels SEDI and DRYDEP, respectively (Kerkweg et al., 2006a), while wet deposition is simulated by the MESSy submodel SCAV (Tost et al., 2006).

A2 Dry deposition and sedimentation

The EMAC parameterization of dry deposition in the submodel DRYDEP is documented in Kerkweg et al. (2006a). Dry deposition is calculated online, considering the effects of Brownian diffusion, impaction and interception onto vegetation, water, bare soil and snow surfaces. Dry deposition on vegetation is calculated using the "big-leaf" approach (Hicks et al., 1987), as parameterized by Slinn (1982) and later modified by Gallagher et al. (2002). Dry deposition on water surfaces is calculated following Slinn and Slinn (1980) over smooth waters and Hummelshøj et al. (1992) over choppy waters. Dry deposition over bare soil and snow surfaces is calculated according to Slinn (1976).

Dry deposition due to surface interactions only occurs in the lowest model layer, as opposed to sedimentation, which occurs throughout the model and is independent of surface characteristics. For these reasons, sedimentation is treated separately in EMAC, in the SEDI submodel (Kerkweg et al., 2006a). The settling velocity is given by the product of the Stokes settling velocity, multiplied by the Cunningham slip correction (Hinds, 1982).

A3 Wet deposition

The wet deposition parameterizations used in EMAC are documented in Tost et al. (2006) and Tost (2006). Aerosol scavenging rates were calculated online, in dependence on cloud droplet and raindrop size, rainfall and snowfall intensity and aerosol diameter.

A3.1 Scavenging during cloud droplet nucleation and growth

The uptake of aerosol particles into cloud droplets due to nucleation on the particles is parameterized by an empirical function for the scavenged fraction, which was derived from measurements presented by Svenningsson et al. (1997) and Martinsson et al. (1999). The nucleation rate for CCN-active particles rises sharply from less than 1% for r_{aer}=0.1 μmto 50% at r_{aer}=0.2 μmand over 99% at r_{aer}=0.4 μm. The particles in this study have a radius of 1 μm, and so are entirely taken up into cloud droplets if assumed to be CCN-active. CCN-inactive particles are not taken up by nucleation scavenging.

A3.2 Scavenging by falling raindrops

To estimate scavenging by falling raindrops (both within and below the cloud), SCAV uses a semi-empirical parameterization of the collision efficiency E first proposed by Slinn (1983), that includes the effects of Brownian diffusion, interception and impaction scavenging. Its applicability has also been demonstrated by Andronache (2003, 2004).

Removal by impaction and interception scavenging during transport to the upper troposphere is inefficient for the 1 μm particles considered in this study. This is because they fall into the so-called "scavenging gap": they are too large for diffusion to be efficient and too small for inertial effects and finite size to be important.

ACPD
9, 10829–10881, 2009

A3.3 Impaction scavenging by frozen hydrometeors

Although scavenging by falling raindrops is inefficient, impaction scavenging by falling snow and ice is significant, which contributes to the large differences in the simulations with and without ice-phase scavenging. The scavenging coefficient for impaction scavenging by snow and ice is set to 0.1.

A3.4 Nucleation scavenging by frozen hydrometeors

The ice content of clouds is represented in EMAC by a single bulk variable. For nucleation scavenging by ice, a constant scavenging ratio is applied (the same approach used in e.g. Stier et al., 2005). For mixed-phase clouds warmer than 238.15 K (−35°C), the scavenging coefficient is set to 0.8; otherwise it is set to 0.05. A smaller fraction of the aerosol is scavenged in mixed-phase clouds than in warm clouds. This has been attributed to the Bergeron-Findeisen effect, which leads to growth of a small number of ice crystals at the expense of the evaporation of a larger number of cloud droplets, which release particles (Henning et al., 2004).

Ice phase scavenging was found to be an important removal process, but it is poorly understood at present and its representation in models is crude. For instance, differential scavenging due to the different ice-nucleating capabilities of particles is not considered in the model. Since bacteria are often good ice nucleators, they may be scavenged at higher rates than other aerosol particles, but this effect could not be considered in the current study. Future work is necessary to understand the sensitivity of simulated aerosol distributions to ice-phase scavenging rates and to develop improved scavenging parameterizations.

A3.5 Large scale clouds, deep convection, and vertical diffusion

In the model set-up used for this study, the vertical transport was parameterized with the submmodel CVTRANS. Cumulus convection is calculated via the mass flux

scheme of Tiedtke (1989) with modifications for penetrative convection according to Nordeng (1994). Stratiform cloud microphysics is calculated using the parameterization of Lohmann and Roeckner (1996) and the statistical cloud cover scheme of Tompkins (2002). The turbulent vertical flux in the boundary layer is calculated according to Roeckner et al. (2003), Chapter 5.

A4 Data handling

Model results were output as averages over each six-hour time interval. In post-processing, this output was averaged to obtain "climatological" monthly mean values for mixing ratios and loss rates in each grid cell[2]. The analysis was done on the basis of the monthly mean data. Finally, ecosystem emission fluxes were adjusted to fit estimated concentrations from the literature. The numerical procedures used are described in Sect. 4.

The inversion analysis was performed using the open-source statistical programming language R and its standard libraries (R Development Core Team, 2008). For the Method 1 fitting, the method of Byrd et al. (1995) was used (as implemented in the *R* statistics function optim), which finds local minima of a single-valued function while satisfying upper and lower boundary conditions on each function argument. In Method 2, the cost function was minimized using a constrained nonlinear optimization function from the *R* statistics package (nlminb), which utilizes the routines from the PORT library developed at AT&T Bell Laboratories (Gay, 1990).

[2]The term "climatological" mean is used here to refer to the mean over a particular month of all years, such as the mean over the Januaries of all three simulation years. It is not intended to imply a long-term, truly climatological average.

Appendix B Ecosystem lumping

The basis for ecosystem classification is the Olson World Ecosystems dataset (Olson, 1992), which is freely available from NOAA at the time of writing (http://www.ngdc.noaa.gov/ecosys/). Ecosystem classes are assigned at each point of a grid with a mixture of 30 min and 10 min spatial resolution. Each class is associated with an integer index from 0 through 73 (inclusive), with 14 of the indices remaining unused.

Because the Olson ecosystem classification was too detailed for the present purposes, the classes were lumped into groups as detailed in Table B1. The geographic distribution of the lumped ecosystems is illustrated in Fig. 1. The data were regridded onto the model grid points using NCREGRID (Jöckel, 2006). For each box of the new grid, NCREGRID returns a vector. Each element of the vector is the fraction of the new grid box covered by one ecosystem from the lumped set (see regridding type IFX in Jöckel, 2006).

Appendix C Tabulated results

See Tables C1–C6.

Acknowledgements. This material is based upon work supported under a National Science Foundation Graduate Research Fellowship (grant number 0633824) awarded to Susannah Burrows. The Max Planck Institute for Chemistry and the International Max Planck Research School on atmospheric chemistry and physics are acknowledged gratefully for hosting Susannah Burrows' research.

The service charges for this open access publication have been covered by the Max Planck Society.

References

Amato, P., Demeer, F., Melaouhi, A., Fontanella, S., Martin-Biesse, A.-S., Sancelme, M., Laj, P., and Delort, A.-M.: A fate for organic acids, formaldehyde and methanol in cloud water: their biotransformation by micro-organisms, Atmos. Chem. Phys., 7, 4159–4169, 2007, http://www.atmos-chem-phys.net/7/4159/2007/. 10848

Andronache, C.: Estimated variability of below-cloud aerosol removal by rainfall for observed aerosol size distributions, Atmos. Chem. Phys., 3, 131–143, 2003, http://www.atmos-chem-phys.net/3/131/2003/. 10851

Andronache, C.: Estimates of sulfate aerosol wet scavenging coefficient for locations in the Eastern United States, Atmos. Environ., 38, 795–804, 2004. 10851

Ariya, P.: Microbiological degradation of atmospheric organic compounds, Geophys. Res. Lett., 29, p. 34, doi:10.1029/2002GL015637, 2002. 10848

Bauer, H., Kasper-Giebl, A., Löflund, M., Giebl, H., Hitzenberger, R., Zibuschka, F., and Puxbaum, H.: The contribution of bacteria and fungal spores to the organic carbon content of cloud water, precipitation and aerosols, Atmos. Res., 64, 109–119, doi:10.1016/S0169-8095(02)00084-4, 2002. 10836, 10863

Bauer, H., Giebl, H., Hitzenberger, R., Kasper-Giebl, A., Reischl, G., Zibuschka, F., and Puxbaum, H.: Airborne bacteria as cloud condensation nuclei, J. Geophys. Res., 108, 4658, doi:10.1029/2003JD003545, 2003. 10848, 10849

Burrows, S. M., Elbert, W., Lawrence, M., and Pöschl, U.: Bacteria in the global atmosphere – Part 1: Review and synthesis of literature data for different ecosystems, Atmos. Chem. Phys. Discuss., 9, 10777–10827, 2009, http://www.atmos-chem-phys-discuss.net/9/10777/2009/. 10830, 10836, 10845, 10847, 10863

Byrd, R., Lu, P., Nocedal, J., and Zhu, C.: A limited memory algorithm for bound constrained optimization, SIAM J. Sci. Stat. Comp., 16, 1190–1208, 1995. 10853

Diehl, K., Simmel, M., and Wurzler, S.: Numerical sensitivity studies on the impact of aerosol properties and drop freezing modes on the glaciation, microphysics, and dynamics of clouds, J. Geophys. Res., 111, 7202, doi:10.1029/2005JD005884, 2006. 10832

Dimmick, R., Wolochow, H., and Chatigny, M.: Evidence for more than one division of bacteria within airborne particles, Appl. Environ. Microb., 38, 642–643, 1979. 10848

Elbert, W., Taylor, P. E., Andreae, M. O., and Pöschl, U.: Contribution of fungi to primary

biogenic aerosols in the atmosphere: wet and dry discharged spores, carbohydrates, and inorganic ions, Atmos. Chem. Phys., 7, 4569–4588, 2007, http://www.atmos-chem-phys.net/7/4569/2007/. 10844, 10847
Enting, I.: Inverse Methods in Global Biogeochemical Cycles, chap. Green's function methods of tracer inversion, American Geophysical Union, 2000. 10837
Franc, G. and DeMott, P.: Cloud Activation Characteristics of Airborne Erwinia carotovora Cells, J. Appl. Meteorol., 37, 1293–1300, 1998. 10849
Gallagher, M., Nemitz, E., Dorsey, J., Fowler, D., Sutton, M., Flynn, M., and Duyzer, J.: Measurements and parameterizations of small aerosol deposition velocities to grassland, arable crops, and forest: Influence of surface roughness length on deposition, J. Geophys. Res., 107(D12), 4154, doi:10.1029/2001JD000817, 2002. 10850
Gay, D.: Usage summary for selected optimization routines, Computing Science Technical Report, AT&T Bell Laboratories, 1990. 10853
Gregory, P.: The microbiology of the atmosphere, Leonard Hill, USA, 1973. 10830
Griffin, D., Garrison, V., Herman, J., and Shinn, E.: African desert dust in the Caribbean atmosphere: Microbiology and public health, Aerobiologia, 17, 203–213, 2001a. 10834
Griffin, D., Kellogg, C., and Shinn, E.: Dust in the Wind: Long Range Transport of Dust in the Atmosphere and Its Implications for Global Public and Ecosystem Health, Global Change & Human Health, 2, 20–33, 2001b. 10834
Griffin, D., Westphal, D., and Gray, M.: Airborne microorganisms in the African desert dust corridor over the mid-Atlantic ridge, Ocean Drilling Program, Leg 209, Aerobiologia, 22, 211–226, 2006. 10863
Harrison, R., Jones, A., Biggins, P., Pomeroy, N., Cox, C., Kidd, S., Hobman, J., Brown, N., and Beswick, A.: Climate factors influencing bacterial count in background air samples, Int. J. Biometeorol., 49, 167–178, 2005. 10836, 10863
Henning, S., Bojinski, S., Diehl, K., Ghan, S., Nyeki, S., Weingartner, E., Wurzler, S., and Baltensperger, U.: Aerosol partitioning in natural mixed-phase clouds, Geophys. Res. Lett., 31, L06101, doi:10.1029/2003GL019025, 2004. 10852
Herlihy, L., Galloway, J., and Mills, A.: Bacterial utilization of formic and acetic acid in rainwater, Atmos. Environ., 21, 2397–2402, 1987. 10848
Hicks, B., Baldocchi, D., Meyers, T., Hosker, R., and Matt, D.: A preliminary multiple resistance routine for deriving dry deposition velocities from measured quantities, Water Air Soil Pollut., 36, 311–330, 1987. 10850

Hinds, W. C.: Aerosol technology: Properties, behavior, and measurement of airborne particles, Wiley-Interscience, New York, USA, 442 pp., 1982. 10850
Hummelshøj, P., Jensen, N., and Larson, S.: Precipitation scavenging and atmosphere-surface exchange, chap. Particle dry deposition to a sea surface, Hemisphere Publishing Corporation, Washington, USA, 1992. 10850
Jaenicke, R.: Abundance of Cellular Material and Proteins in the Atmosphere, Science, 308, p. 73, doi:10.1126/science.1106335, 2005. 10844, 10847
Jöckel, P.: Technical note: Recursive rediscretisation of geo-scientific data in the Modular Earth Submodel System (MESSy), Atmos. Chem. Phys., 6, 3557–3562, 2006, http://www.atmos-chem-phys.net/6/3557/2006/. 10854
Jöckel, P., Sander, R., Kerkweg, A., Tost, H., and Lelieveld, J.: Technical Note: The Modular Earth Submodel System (MESSy) - a new approach towards Earth System Modeling, Atmos. Chem. Phys., 5, 433–444, 2005, http://www.atmos-chem-phys.net/5/433/2005/. 10832
Jöckel, P., Tost, H., Pozzer, A., Brühl, C., Buchholz, J., Ganzeveld, L., Hoor, P., Kerkweg, A., Lawrence, M. G., Sander, R., Steil, B., Stiller, G., Tanarhte, M., Taraborrelli, D., van Aardenne, J., and Lelieveld, J.: The atmospheric chemistry general circulation model ECHAM5/MESSy1: consistent simulation of ozone from the surface to the mesosphere, Atmos. Chem. Phys., 6, 5067–5104, 2006, http://www.atmos-chem-phys.net/6/5067/2006/. 10832
Jöckel, P., Kerkweg, A., Buchholz-Dietsch, J., Tost, H., Sander, R., and Pozzer, A.: Technical Note: Coupling of chemical processes with the Modular Earth Submodel System (MESSy) submodel TRACER, Atmos. Chem. Phys., 8, 1677–1687, 2008, http://www.atmos-chem-phys.net/8/1677/2008/. 10849
Jones, A. M. and Harrison, R. M.: The effects of meteorological factors on atmospheric bioaerosol concentrations – a review, Sci. Total Environ., 326, 151–180, 2004. 10830, 10845
Kasibhatla, P., Heimann, M., Rayner, P., Mahowald, N., Prinn, R., and Hartley, D.(eds.): Inverse Methods in Global Biogeochemical Cycles, American Geophysical Union, 2000. 10836
Kerkweg, A., Buchholz, J., Ganzeveld, L., Pozzer, A., Tost, H., and Jöckel, P.: Technical Note: An implementation of the dry removal processes DRY DEPosition and SEDImentation in the Modular Earth Submodel System (MESSy), Atmos. Chem. Phys., 6, 4617–4632, 2006a. 10850
Kerkweg, A., Sander, R., Tost, H., and Jöckel, P.: MESSy Emissions Users Manual, Air Chem-

istry Department, Max-Planck Institute of Chemistry, PO Box 3060, 55020 Mainz, Germany, online available: akerkweg@mpch-mainz.mpg.de, 2006b. 10850
Kerkweg, A., Sander, R., Tost, H., and Jöckel, P.: Technical note: Implementation of prescribed (OFFLEM), calculated (ONLEM), and pseudo-emissions (TNUDGE) of chemical species in the Modular Earth Submodel System (MESSy), Atmos. Chem. Phys., 6, 3603–3609, 2006c. 10850
Lighthart, B. and Shaffer, B. T.: Bacterial flux from chaparral into the atmosphere in mid-summer at a high desert location, Atmos. Environ., 28, 1267–1274, 1994. 10863
Lin, S. and Rood, R.: Multidimensional Flux-Form Semi-Lagrangian Transport Schemes, Monthly Weather Review, 124, 2046–2070, 1996. 10850
Lohmann, U. and Roeckner, E.: Design and performance of a new cloud microphysics scheme developed for the ECHAM general circulation model, Clim. Dynam., 12, 557–572, 1996. 10853
Martinsson, B., Frank, G., Cederfelt, S., Swietlicki, E., Berg, O., Zhou, J., Bower, K., Bradbury, C., Birmili, W., Stratmann, F., et al.: Droplet nucleation and growth in orographic clouds in relation to the aerosol population, Atmos. Res., 50, 289–315, 1999. 10851
Möhler, O., DeMott, P. J., Vali, G., and Levin, Z.: Microbiology and atmospheric processes: the role of biological particles in cloud physics, Biogeosciences, 4, 1059–1071, 2007, http://www.biogeosciences.net/4/1059/2007/. 10832
Morris, C., Georgakopoulos, D., and Sands, D.: Ice nucleation active bacteria and their potential role in precipitation, J. Phys. IV France, 121, 87–103, 2005. 10848
Nordeng, T. E.: Extended versions of the convective parameterization scheme at ECMWF and their impact on the mean and transient activity of the model in the tropics., Tech. Rep. Technical Memorandum 206, ECMWF, Reading, UK, 1994. 10853
Olson, J.: World ecosystems (WE1. 4): Digital raster data on a 10 minute geographic 1080 (2160 grid square), Global Ecosystem Database, Version, 1, 1992. 10833, 10854, 10866, 10873
Prescott, L., Harley, J., and Klein, D.: Microbiology, Wm. C. Brown Publishers, Dubuque, IA, USA, third edn., 37–41, 1996. 10846
R Development Core Team: R: A Language and Environment for Statistical Computing, version 2.7.2, R Foundation for Statistical Computing, Vienna, Austria, online available at: http://www.R-project.org, ISBN 3-900051-07-0, 2008. 10853
Roeckner, E., Bauml, G., Bonaventura, L., Brokopf, R., Esch, M., Giorgetta, M., Hagemann,

S., Kirchner, I., Kornblue, L., Manzini, E., et al.: The atmospheric general circulation model ECHAM5. Part 1: Model description, Tech. Rep. 349, Max Planck Institute for Meteorology, Hamburg, Germany, 2003. 10832, 10853
Roedel, W.: Physik unserer Umwelt, Die Atmosphäre, Berlin Heidelberg, Germany, 1992. 10833
Sands, D., Langhans, V., Scharen, A., and Desmet, G.: The association between bacteria and rain and possible resultant meteorological implications, Idojaras (Budapest), 86, 148–152, 1992. 10848
Sattler, B., Puxbaum, H., and Psenner, R.: Bacterial growth in supercooled cloud droplets, Geophys. Res. Lett., 28, 239–242, doi:10.1029/2000GL011684, 2001. 10848
Schnell, R. and Vali, G.: World-wide source of leaf-derived freezing nuclei, Nature, 246, 212–213, 1973. 10848
Schnell, R. and Vali, G.: Biogenic Ice Nuclei: Part I. Terrestrial and Marine Sources, J. Atmos. Sci., 33, 1554–1564, 1976. 10849
Schulz, H. and Jorgensen, B.: Big Bacteria, Annu. Rev. Microbiol., 55, 105–137, 2001. 10846
Schulz, M., Balkanski, Y. J., Guelle, W., and Dulac, F.: Role of aerosol size distribution and source location in a three-dimensional simulation of a Saharan dust episode tested against satellite-derived optical thickness, J. Geophys. Res., 103, 10579–10592, doi:10.1029/97JD02779, 1998. 10835
Shaffer, B. T. and Lighthart, B.: Survey of Culturable Airborne Bacteria at Four Diverse Locations in Oregon: Urban, Rural, Forest, and Coastal, Microb. Ecol., 34, 167–177, 1997. 10863
Slinn, S. and Slinn, W.: Predictions for Particle Deposition on Natural Waters, Atmos. Environ., 14, 1013–1016, doi:10.1016/0004-6981(80)90032-3, 1980. 10850
Slinn, W.: Predictions for particle deposition to vegetative canopies, Atmos. Environ., 16(7), 1785–1794, doi:10.1016/0004-6981(82)90271-2, 1982. 10850
Slinn, W.: Precipitation Scavenging, Dry Deposition and Resuspension, chap. chap. 11, Precipitation Scavenging, United States Dept. of Energy, 1983. 10851
Slinn, W. G. N.: Atmosphere-surface exchange of particulate and gaseous pollutants, chap. Dry deposition and resuspension of aerosol particles – a new look at some old problems, US DOE Tech. Info. Center, Oak Ridge, TN, USA, 1976. 10850
Stier, P., Feichter, J., Kinne, S., Kloster, S., Vignati, E., Wilson, J., Ganzeveld, L., Tegen, I., Werner, M., Balkanski, Y., Schulz, M., Boucher, O., Minikin, A., and Petzold, A.: The aerosol-

climate model ECHAM5-HAM, Atmos. Chem. Phys., 5, 1125–1156, 2005, http://www.atmos-chem-phys.net/5/1125/2005/. 10852

Sun, J. and Ariya, P. A.: Atmospheric organic and bio-aerosols as cloud condensation nuclei (CCN): A review, Atmos. Environ., 40, 795–820, doi:10.1016/j.atmosenv.2005.05.052, 2006. 10848

Svenningsson, B., Hansson, H., Martinsson, B., Wiedensohler, A., Swietlicki, E., Cederfelt, S., Wendisch, M., Bower, K., Choularton, T., and Colvile, R.: Cloud droplet nucleation scavenging in relation to the size and hygroscopic behaviour of aerosol particles, Atmos. Environ., 31, 2463–2475, 1997. 10851

Tiedtke, M.: A Comprehensive Mass Flux Scheme for Cumulus Parameterization in Large-Scale Models, Mon. Weather Rev., 117, 1779–1800, doi:10.1175/1520-0493(1989)117⟨1779:ACMFSF⟩2.0.CO;2, 1989. 10853

Tilley, R., Eamus, D., and Ho, J.: Background Bioaerosols and Aerosols at Two Sites in Northern Australia: Preliminary Measurements, Tech. rep., DSTO Aeronautical and Maritime Research Laboratory, Victoria, Australia, 2001. 10863

Tompkins, A.: A prognostic parameterization for the subgrid-scale variability of water vapor and clouds in large-scale models and its use to diagnose cloud cover., J. Atmos. Sci., 59, 1917–1942, 2002. 10853

Tong, Y. and Lighthart, B.: Diurnal Distribution of Total and Culturable Atmospheric Bacteria at a Rural Site, Aerosol Sci. Tech., 30, 246–254, 1999. 10836, 10863

Tost, H.: Global Modelling of Cloud, Convection and Precipitation Influences on Trace Gases and Aerosols, Ph.D. thesis, Rheinische Friedrich-Wilhelms-Universitat Bonn, Germany, online available at: http://hss.ulb.uni-bonn.de/diss_online, 2006. 10851

Tost, H., Jöckel, P., Kerkweg, A., Sander, R., and Lelieveld, J.: Technical note: A new comprehensive SCAVenging submodel for global atmospheric chemistry modelling, Atmos. Chem. Phys., 6, 565–574, 2006, http://www.atmos-chem-phys.net/6/565/2006/. 10850, 10851

Wolfenbarger, D. O.: Dispersion of Small Organisms. Distance Dispersion Rates of Bacteria, Spores, Seeds, Pollen, and Insects; Incidence Rates of Diseases and Injuries, Am. Midl. Nat., 35, 1–152, 1946. 10848

Table 1. Removal processes included in the three sensitivity simulations.

	Sedimentation	Dry deposition	Impaction and interception scavenging	Cloud droplet nucleation	Uptake by diffusion	Ice-phase scavenging (impaction and nucleation)
CCN-ACTIVE	+	+	+	+	+	+
CCN-INACTIVE	+	+	+	–	+	+
NO-ICE-SCAV	+	+	+	–	+	–

ACPD
9, 10829–10881, 2009

Table 2. Global mean particle lifetimes by scavenging characteristics and source ecosystem (days).

Simulation	global	coastal	crops	deserts	forests	grasslands	landice	seas	shrubs	tundra	wetlands
CCN-ACTIVE	2.5	3.4	3.4	6.2	2.7	3.1	6.3	1.8	4.6	3.9	3
CCN-INACTIVE	5.1	6.7	6.5	9.2	6	7	8.1	4.4	7.7	6.2	6.4
NO-ICE-SCAV	96	102	104	114	101	107	71	95	109	88	102

Table 3. Estimates of total mean bacterial concentration in near-surface air of various ecosystem types, from Burrows et al. (2009).

Ecosystem	Best estimate[a] (m^{-3})	Low estimate[a] (m^{-3})	High estimate (m^{-3})	Percent uncertainty[b]
coastal[c]	7.6×10^4	2.3×10^4	1.3×10^5	300
crops[c]	1.1×10^5	4.1×10^4	1.7×10^5	81
deserts[d,e]	(*1×10^4*)	1.6×10^2	3.8×10^4	380
forests[f]	5.6×10^4	3.3×10^4	8.8×10^4	100
grasslands[c,g]	1.1×10^5	2.5×10^4	8.4×10^5	290
land ice[h,i]	(*5×10^3*)	(*1×10^1*)	1×10^4	200
seas[c,g,j]	1×10^4	1×10^1	8×10^4	800
shrubs[f,g]	3.5×10^5	1.2×10^4	8.4×10^5	240
tundra[e,g,k]	1.2×10^4	(*1×10^1*)	5.6×10^4	470
wetlands[l]	9×10^4	2×10^4	8×10^5	870

[a] Additional values have been assumed for fields left blank by Burrows et al. (2009); these are denoted by parentheses and italic font.
[b] Percent uncertainties are calculated as best/(high – low)×100.
[c] Harrison et al. (2005)
[d] Lighthart and Shaffer (1994)
[e] Assumed the same best estimate as for seas.
[f] Shaffer and Lighthart (1997)
[g] Tong and Lighthart (1999); Tilley et al. (2001)
[h] Bauer et al. (2002)
[i] Estimated low value for seas taken as lower bound, average of high and low values taken as best estimate.
[j] Griffin et al. (2006)
[k] Estimated low value for seas taken as lower bound.
[l] Assumed to be within bounds of best estimates in coastal and grassland/crops regions.

Table 4. Summary of estimated emissions of bacteria from all ecosystems (Method 2 best fit).

	Area (km^{-2})	Best fit flux	Global emissions (cells/year)	Global emissions (Gg/year)
coastal	809608			
crops	15511990	593	2.90e+23	152
deserts	18916147			
forests	35928050			
grasslands	10954813	1123	3.88e+23	203
landice	15622994	8	3.92e+21	2.1
seas	362871034			
shrubs	29389469	520	4.82e+23	252
tundra	16900928			
wetlands	2877473			
SUM	509782505	2243	1.16e+24	610

Table 5. Simulated global bacteria with adjusted emission fluxes (Method 2 positive best fit) and with homogeneous fluxes normalized to the global emissions.

		Adjusted emissions	Homogeneous emissions
Mean surface concentration (cells m^{-3})	Overall	2.3×10^{4}	1.9×10^{4}
	Over land	6.6×10^{4}	2.7×10^{4}
	Over seas	5.7×10^{3}	1.6×10^{4}
Mean emissions (cells m^{-2} s^{-1})	From land	250	72
	From seas	0	72
Mean global load (cells)		1.7×10^{22}	1.3×10^{26}
Mean global load (Gg)		9.1	5.6
Mean lifetime (days)		5.5	3.3
Global emissions (cells $year^{-1}$)		1.16×10^{24}	1.16×10^{24}
Global emissions (Gg $year^{-1}$)		610	610

ACPD
9, 10829–10881, 2009

Table B1. Lumping of Olson ecosystem classes. Original classification from Olson (1992).

Lumped group number	Lumped group name	Lumped group description	Olson number	Olson code	Olson description
0	seas	Oceans, Seas, Inland Waters	0	(none)	Waters, including ocean and Inland Waters
1	shrubs	Shrubs and scrubs (non-desert)	16	BES	Broadleaf Evergreen Scrub, commonly with 46 and 47
			40	CGS	Cool grass/shrub, showy in most years
			41	MGS	Mild/warm/hot grass/shrub
			46	MES	Mediterranean-type Evergreen (mostly) broadleaved Scrub and forest relics
			47	DHS	Dry or highland scrub, or open woodland
			49	HVI	Hot-mild volcanic "islands" (Galapagos), with local denser forest on some older lava flows but wide areas of sparse cover on recent lavas
			59	STW	Succulent and Thorn Woods or scrub is widespread
2	forests	Forests (temperate, tropical and boreal)	6	TBE	Temperate/Tropical-montane Broadleaf Evergreen covers warm temperate or montane broadleaf evergreen forest (Africa only)
			20	SRC	Snowy, rainy coastal conifer
			21	MBC	Main Boreal conifer forest, closed or open
			22	SNB	Snowy non-Boreal conifer forest
			23	CDF	Conifer/deciduous, snow persisting in winter
			24	TBC	Temperate Broadleaf/Conifer forest: with deciduous and/or evergreen hardwood trees
			25	SDF	Snowy Deciduous Forest, i.e. Summergreen (=cold-deciduous) types
			26	TBF	Temperate broad-leaf forest: deciduous, semideciduous, and some temperate-subtropical broadleaf evergreen types that are least active in winter.
			27	NSC	Non-snowy conifer forest
			28	TMC	Tropical montane complexes, typically evergreen, including dwarfed ("elfin") forest, opening to grass, or tall or short forbs (puna, paramo)
			29	TBS	Tropical Broadleaf Seasonal, with dry or cool season
			32	RGD	Rain-green (drought-deciduous) or very seasonal dry evergreen forests to open woodlands, very frequently burned.
			33	TRF	Tropical Rain Forest
			48	DEW	Dry Evergreen Woodland or low forest, mapped mostly in interior Australia and South America
			54	TER	Temperate Evergreen Rainforest (e.g., in Chile)
			56	FFR	Forest/Field complex with Regrowth after disturbances, mixed with crops and/or other non-wooded lands
			57	SFF	Snowy Forest/Field, commonly openings are pasture and/or mires
3	deserts	Arid and semiarid deserts	8	DMB	Desert, mostly bare stone, clay or sand
			50	SDB	Sand Desert, partly Blowing dunes
			71	SSF	Salt/soda flats desert,playas, occasionally with intermittent lakes
			2	SSG	Short or Sparse Grass/shrub of semiarid climates
			51	SDS	SemiDesert/Desert Scrub/succulent/sparse grass
			52	CSS	Cool/cold shrub semidesert/steppe
4	landice	Land ice and polar deserts	17	ICE	Antarctic ice cap
			69	PDL	Polar desert with rock Lichens, locally abundant or productive (even between mineral grains) but provide little food. Animals import residues for localized humus
			70	GLA	Glaciers in polar or alpine complex, with rock fringes
5	crops	Croplands	30	CFC	Cool Farmland: Settlements, more or less snowy
			31	MFS	Mild/hot farmland & settlements
			36	PRA	Paddy rice and associated land mosaics
			37	WCI	Warm/hot cropland, Irrigated extensively
			38	CCI	Cool cropland with Irrigation of variable extent
			39	CCP	Cold cropland and pasture, irrigated locally
6	wetlands	Wetlands	44	MBF	Mires, including peaty Bogs and Fens (mostly in high latitudes)
			45	MOS	Marsh or other swampy wetlands, includes various transitions to or mixtures with trees
			72	MSM	Mangrove and non-saline swamps and tidal Mudflats (Africa only)
7	coastal	Coastal regions, islands	65	CNW	Coastal: NorthWest quadrant near most land
			66	CNE	Coastal: NorthEast quadrant near most land
			67	CSE	Coastal: SouthEast quadrant near most land
			68	CSW	Coastal: SouthWest quadrant near most land
			73	ISL	Islands and shore waters in oceans and/or lakes (Elba Island)
8	grasslands	Grasslands and Savanna	43	SGW	Savanna/Grass, seasonal woods: Trees or shrubs above grass groundcover may be interspersed on many scales in savana belts of varying drought duration and high fire frequency
			55	SFW	Snowy Field/Woods complex
			58	FWG	Field/Woods with Grass and/or Cropland
9	tundra	Tundras and Taigas	42	CSM	Cold steppe/meadow +/- larch woods (in Siberia), scrub (Bering sea) or tundra (Tibetan highland)
			53	TUN	Tundra (polar, alpine)
			60	SDT	Southern Dry Taiga or similar aspen/birch with northern and/or mountain conifers
			61	LT	Larch Taiga with deciduous conifer
			62	NMT	Northern or maritime taiga typifies a wide latitude belt or a narrow altitude belt above denser forest or woodland
			63	WTM	Wooded tundra margin or mountain scrub/meadow
			64	HMW	Heath and Moorland, wild or artificially managed, as by burning and/or grazing. Can include wetland (44–45) interspersed with drier heath, with dwarfed or taller, commonly dense scrub on peat or sand.

ACPD
9, 10829–10881, 2009

Table C1. Weighting matrix **W**: mean surface concentrations of ecosystem tracers, calculated assuming an emission flux of 1 cell m^{-2} s^{-1}. The source ecosystems are listed across the top, destination ecosystems on the left.

	coastal	crops	deserts	forests	grasslands	landice	seas	shrubs	tundra	wetlands
crops	2.80	76.89	21.14	55.88	34.88	0.90	70.77	26.99	5.51	2.62
deserts	2.07	11.91	353.15	9.15	5.24	0.33	45.52	48.22	1.16	0.92
forests	1.73	35.32	19.29	113.00	42.92	0.69	59.41	24.73	6.84	5.40
grasslands	1.73	29.83	48.90	52.89	131.80	0.24	47.39	49.55	1.04	3.45
landice	0.19	0.13	0.19	0.51	0.04	593.03	30.85	0.28	1.68	0.07
seas	1.23	6.25	8.13	7.53	3.33	11.04	189.07	8.29	2.55	0.80
shrubs	2.11	19.59	130.90	24.38	30.89	0.27	50.09	149.05	1.40	3.64
tundra	1.34	19.88	1.44	57.81	3.41	5.20	48.63	7.27	63.98	0.71
wetlands	3.34	22.61	54.25	72.51	43.44	0.10	115.32	45.43	0.37	29.95

ACPD
9, 10829–10881, 2009

Table C2. Modelled concentrations from fits to literature estimates: low, best and high estimate.

	Method 1 Low	Method 1 Best	Method 1 High	Method 2 Low	Method 2 Best	Method 2 High
coastal	21 424	59 921	198 680	22 995	60 088	96 541
crops	38 197	100 000	196 097	40 994	98 788	77 135
deserts	5957	36 760	145 131	6347	38 006	38 009
forests	39 299	78 843	219 389	40 253	81 993	88 010
grasslands	105 891	168 264	534 375	109 995	191 435	170 217
landice	71	5465	9923	69	4984	9921
seas	3661	11 901	85 263	3803	11 841	24 257
shrubs	27 407	115 704	468 911	28 049	123 759	118 073
tundra	5607	20 824	53 949	6187	19 435	33 264
wetlands	44 920	92 999	351 015	38 635	85 793	210 090

Table C3. Initial guess, exact solution and fluxes from constrained fits to the literature estimates (Low, Best and High). Flux vectors are listed for two different fitting methods, a constrained least-squares fit (Method 1) and a maximum-likelihood fit with penalties for exceeding high and low literature values (Method 2).

	Initial	Exact	Low 1	Best 1	High 1	Low 2	Best 2	High 2	Area (sq km)
coastal	10	−4238	11	0	0	77	0	2137	809 608
crops	400	705	140	692	0	170	593	134	15 511 990
deserts	30	−302	0	0	0	0	0	0	18 916 147
forests	100	−593	0	0	0	0	0	0	35 928 050
grasslands	800	1249	764	926	2993	795	1123	937	10 954 813
landice	10	10	0	8.7	0	0	8	12	15 622 994
seas	10	−38	0	0	281	0	0	52	362 871 034
shrubs	200	2440	0	481	2364	0	520	421	29 389 469
tundra	20	289	0	0	172	0	0	245	16 900 928
wetlands	500	−441	285	510	2711	0	0	4474	2 877 473

Table C4. Cross-correlations of columns in Table C1, demonstrating the correlations between the make-up of the aerosol in different ecosystem regions. This table is visualized in Fig. 4.

	coastal	crops	deserts	forests	grasslands	landice	seas	shrubs	tundra	wetlands
coastal	1.00									
crops	0.24	1.00								
deserts	−0.08	−0.21	1.00							
forests	−0.05	0.51	−0.32	1.00						
grasslands	−0.04	0.33	−0.11	0.42	1.00					
landice	−0.25	−0.43	−0.22	−0.42	−0.29	1.00				
seas	0.56	−0.03	−0.28	−0.15	−0.20	−0.32	1.00			
shrubs	0.03	0.03	0.42	−0.07	0.25	−0.33	−0.20	1.00		
tundra	−0.11	−0.02	−0.25	0.21	−0.27	−0.13	−0.19	−0.30	1.00	
wetlands	0.08	0.05	−0.06	0.43	0.21	−0.21	0.21	0.13	−0.21	1.00

ACPD
9, 10829–10881, 2009

Table C5. Ensemble results for total number of cells emitted to the atmosphere per year. Ensemble calculations as in Fig. 8.

	Exact solution	Weighted best fit with positive constraint
Minimum	−8.02e+23	3.60e+23
1%ile	−4.28e+23	5.18e+23
5%ile	4.13e+22	7.68e+23
10%ile	3.87e+23	8.71e+23
25%ile	1.15e+24	1.11e+24
50%ile	2.76e+24	1.31e+24
75%ile	5.34e+24	1.63e+24
90%ile	7.16e+24	2.42e+24
95%ile	7.74e+24	2.84e+24
99%ile	8.39e+24	3.64e+24
Maximum	8.81e+24	4.42e+24

Table C6. Ensemble results for total mass of bacteria emitted to the atmosphere per year, in Gg. Ensemble calculations as in Fig. 8.

	Exact solution	Weighted best fit with positive constraint
Minimum	−420	188
1%ile	−224	271
5%ile	22	402
10%ile	203	456
25%ile	603	580
50%ile	1444	686
75%ile	2795	852
90%ile	3750	1266
95%ile	4050	1488
99%ile	4393	1907
Maximum	4613	2314

ACPD
9, 10829–10881, 2009

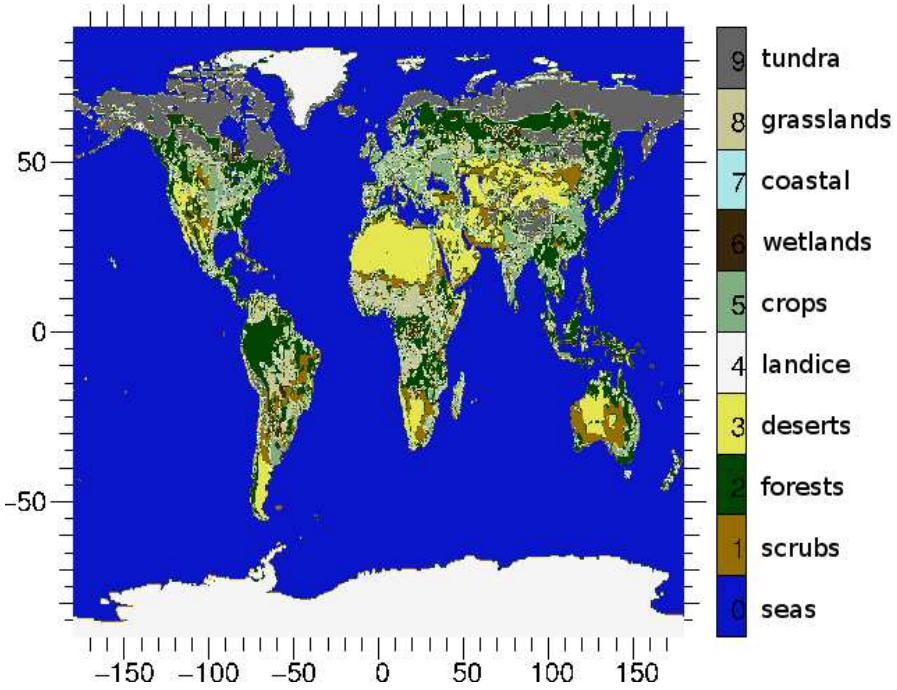

Fig. 1. Lumped ecosystem classes, based on the Olson World Ecosystems (Olson, 1992). For details of lumping, see Table C.

ACPD
9, 10829–10881, 2009

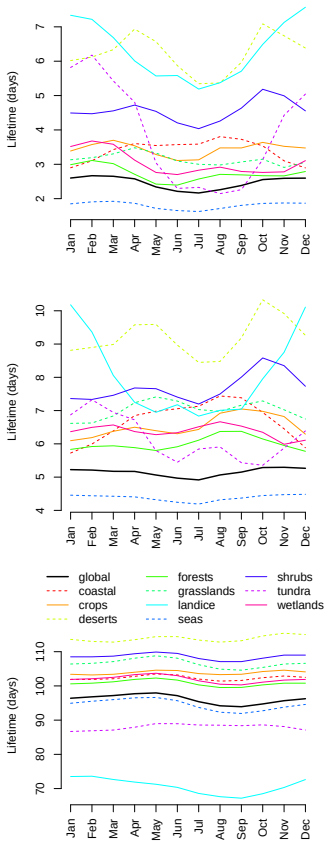

Fig. 2. Global mean lifetimes calculated from climatological monthly mean of global load and fixed (constant) emission flux. Top: CCN-ACTIVE; Middle: CCN-INACTIVE; bottom: NO-ICE-SCAV.

ACPD
9, 10829–10881, 2009

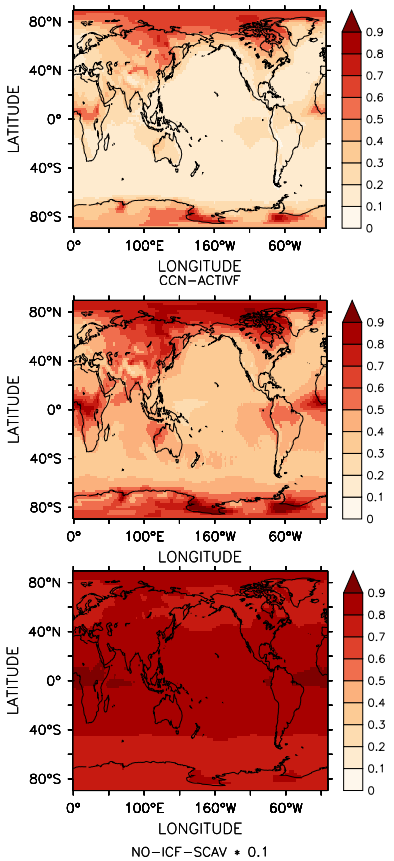

Fig. 3. Column densities (10^{28} m^{-2}) of 1 μm diameter aerosol particles representing bacteria, homogeneously emitted at a rate of 1 m^{-2} s^{-1}. Note that NO-ICE-SCAV is multiplied by a factor of 0.1.

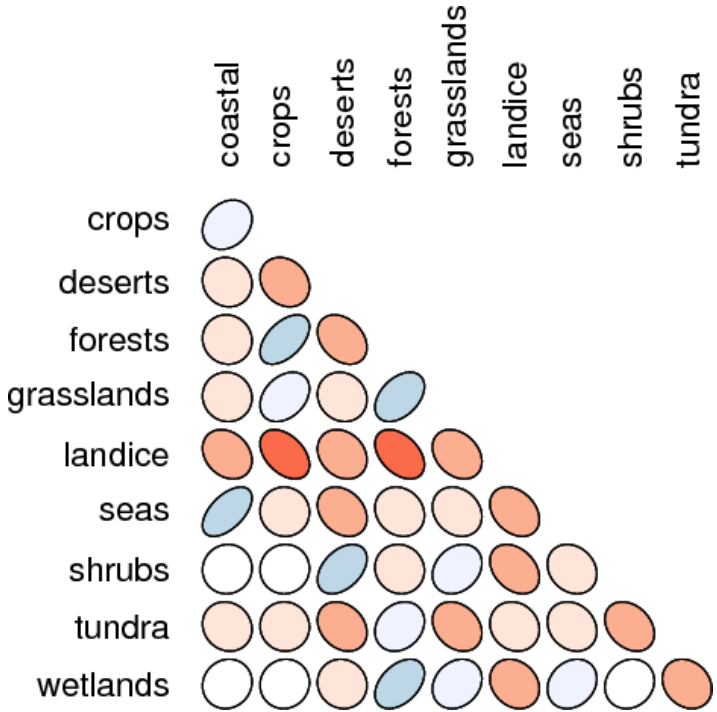

Fig. 4. Cross-correlation of ecosystem tracer distributions by concentration in near-surface air of source ecosystem (correlation of lines of Fig. 5 and columns of Table C4). Greater elongation of ellipses and higher color saturation indicates higher correlation. Blue, right-tilting ellipses represent positive correlations, while red, left-tilting ellipses represent negative values.)

ACPD
9, 10829–10881, 2009

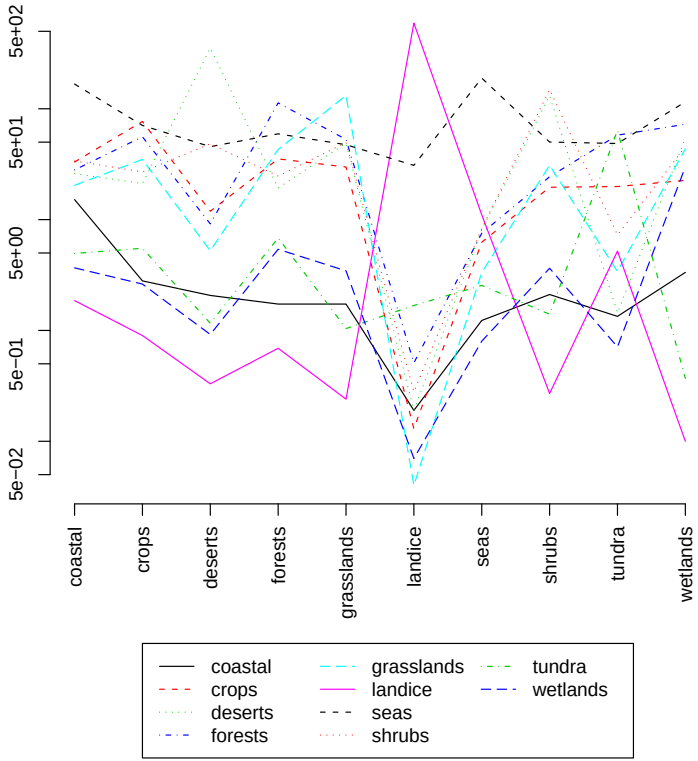

Fig. 5. Each line represents the impact on modelled concentrations of model fluxes from one ecosystem, i.e. a single column of Table C1. Note that the vertical scale is logarithmic.

ACPD
9, 10829–10881, 2009

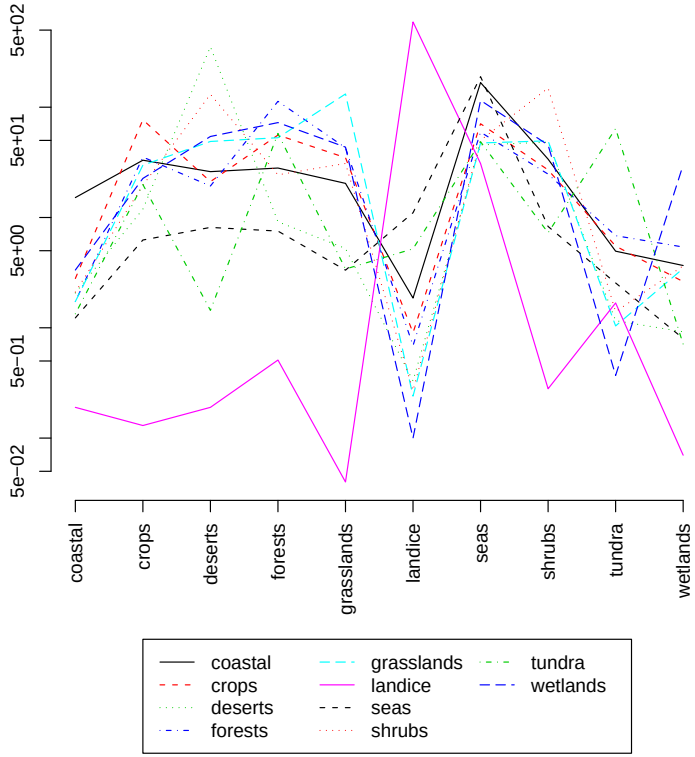

Fig. 6. Each line represents the sensitivity of the flux estimate in one ecosystem to concentration estimates, i.e. a single row of Table C1. Note that the vertical scale is logarithmic.

ACPD
9, 10829–10881, 2009

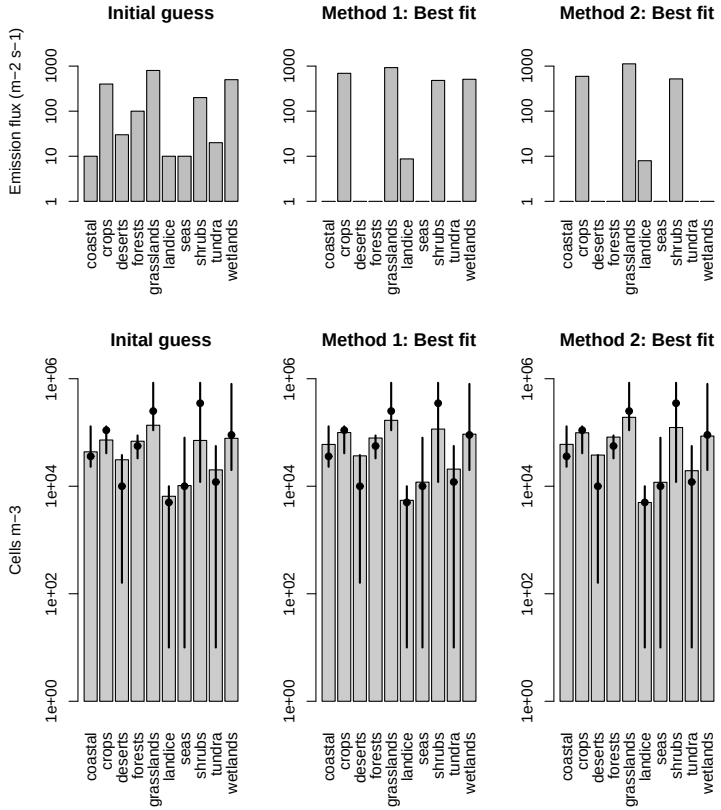

Fig. 7. Top: emission fluxes by ecosystem; bottom: corresponding mean concentrations of particles in near-surface air by ecosystem; dots are best literature estimates, with range shown by vertical lines. Note that the vertical scales are logarithmic. Left: initial guess; center: constrained least-squares; right: maximum likelihood (see text).

ACPD
9, 10829–10881, 2009

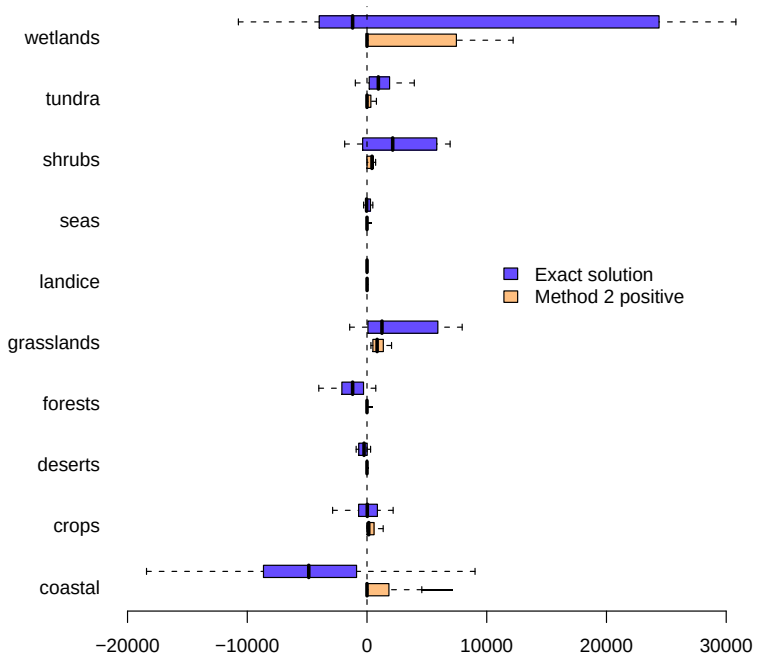

Fig. 8. Statistical summary of an ensemble of flux estimates, in cells $m^{-2}\,s^{-1}$, for the exact fit and the Method 2 best fit with fluxes constrained to be positive. Fitting was performed for an ensemble of state vectors with elements selected from the low, middle and high literature estimates of the mean concentrations in each ecosystem (Table 3), resulting in 3^{10}=59049 ensemble members. Boxes show the 25%-ile to 75%-ile of the estimated fluxes. The vertical line within each box is the corresponding fit to the best literature estimate, which in every case coincides with the median of the ensemble estimates. The dashed lines extend to the farthest point from the median, as long as the distance from the end of the box to that point is no more than 1.5 times the interquartile. Points beyond the dashed line are plotted individually as single dots, giving the appearance of a solid line where closely spaced (coastal, Method 2 positive).

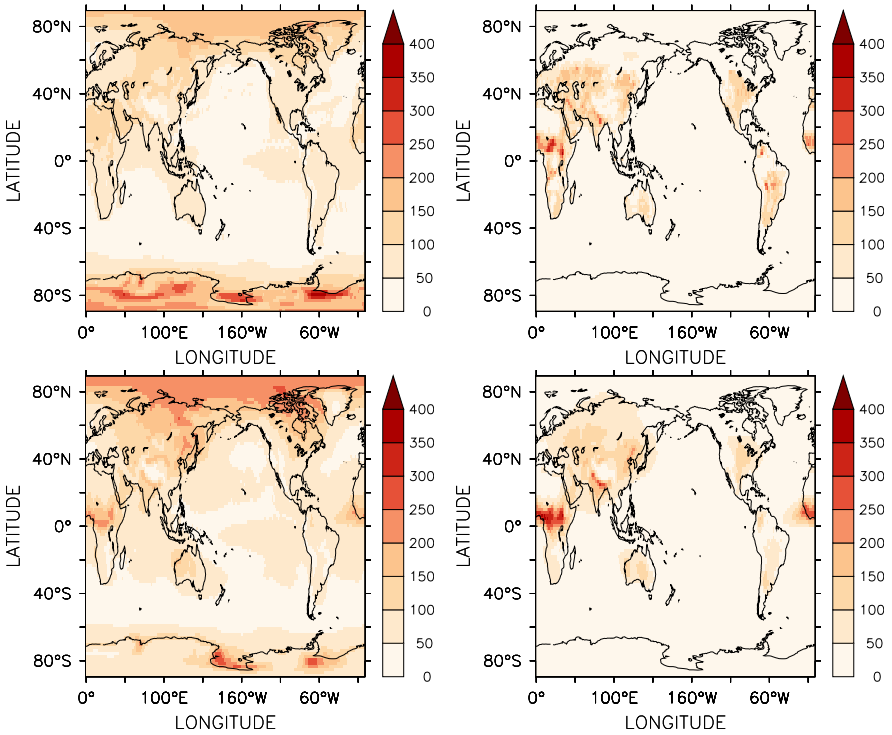

Fig. 9. Top: modelled concentration of bacterial cells in near-surface air (10^3 m^{-3}). Bottom: modelled column density of bacterial cells (10^6 m^{-2} s^{-1}. Figures are based on the CNN-ACTIVE simulation, with homogeneous emissions of 250 m^{-2} s^{-1} in all ecosystems (left) or Method 2 positive best-fit emissions from Appendix C, Table C3 (right).

ACPD
9, 10829–10881, 2009